

Brain Tumor Synthetic Segmentation in 3D Multimodal MRI Scans

Mohammad Hamghalam^{1,2}[0000-0003-2543-0712], Baiying Lei¹, and Tianfu Wang¹

¹ National-Regional Key Technology Engineering Laboratory for Medical Ultrasound, Guangdong Key Laboratory for Biomedical Measurements and Ultrasound Imaging, School of Biomedical Engineering, Health Science Center, Shenzhen University, Shenzhen, China, 518060.

² Faculty of Electrical, Biomedical and Mechatronics Engineering, Qazvin Branch, Islamic Azad University, Qazvin, Iran.
m.hamghalam@gmail.com
{leiby,tfwang}@szu.edu.cn

Abstract. The magnetic resonance (MR) analysis of brain tumors is widely used for diagnosis and examination of tumor subregions. The overlapping area among the intensity distribution of healthy, enhancing, non-enhancing, and edema regions makes the automatic segmentation a challenging task. Here, we show that a convolutional neural network trained on high-contrast images can transform the intensity distribution of brain lesions in its internal subregions. Specifically, a generative adversarial network (GAN) is extended to synthesize high-contrast images. A comparison of these synthetic images and real images of brain tumor tissue in MR scans showed significant segmentation improvement and decreased the number of real channels for segmentation. The synthetic images are used as a substitute for real channels and can bypass real modalities in the multimodal brain tumor segmentation framework. Segmentation results on BraTS 2019 dataset demonstrate that our proposed approach can efficiently segment the tumor areas. In the end, we predict patient survival time based on volumetric features of the tumor subregions as well as the age of each case through several regression models.

Keywords: Tumor segmentation · Synthetic image · GAN · Regression model · Overall survival.

1 Introduction

Glioma is the most aggressive and widespread tumor is grouped into low-grade gliomas (LGGs) and high-grade gliomas (HGGs). Multimodal MR channels in BraTS 2019 datasets [4,2,1,3,13], included of FLAIR, T1, T1c, and T2, are routinely used to segment internal parts of the tumor, i.e., whole tumor (WT), tumor core (TC), and enhancing tumor (ET). Several segmentation approaches have been proposed to segment regions of interest through classic [7,8,18,17] and

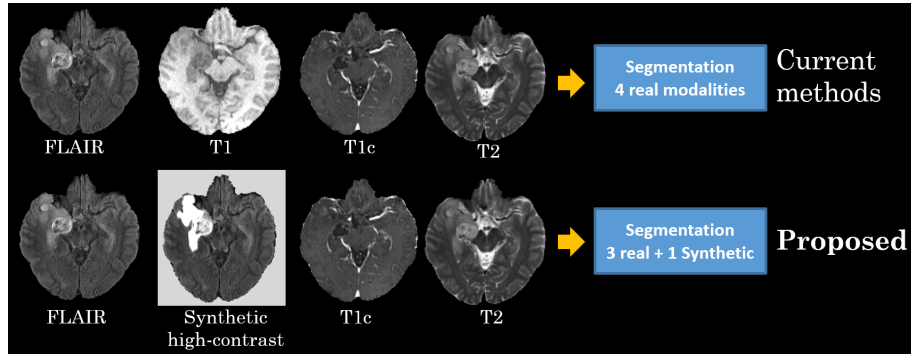


Fig. 1. The pipeline outlines the steps in the current (top) and proposed synthetic (bottom) segmentation techniques. We displace the real T1 channels with the synthetic image.

modern machine learning methods, especially brain tumor segmentation techniques [10,14].

The focus of current research is to form a generator that increases the contrast within subregions of the brain tissue. The generator, which is a deep neural network model, employs a real channel as input to produce the synthetic one. Our framework comprises two stages: (1) we generate high tissue contrast images based on FLAIR sequence in our convolutional neural network (CNN) model, (2) we train a 3D fully convolutional network (FCN) [5,9,16,12] based on the synthetic images to segment region of interests.

2 Method

Our goal is to segment tumor subregions based on multimodal 3D magnetic resonance (MR) volumes. Fig.1 demonstrates an overview of the proposed method based on synthetic high-contrast images. In contrast to the current methods, we use both real and synthetic volumes for the segmentation task. Following, we first introduce the synthetic image generator module, based on the generative adversarial networks (GANs) model [6], and then 3D FCN architecture for segmentation is discussed.

2.1 Synthetic Image Generator

We extend the image-to-image translation method [11] to deal with the synthesis of high-contrast 2D images. Our model trains on high-contrast images, building based on manual labels, in an adversarial framework. The synthesis model contains a Generator, based on the 2D-U-Net [15], and a Discriminator, build on 2D FCN network. Fig. illustrates the image translation framework, where both the generator and the discriminator blocks are trained on FLAIR with a patch

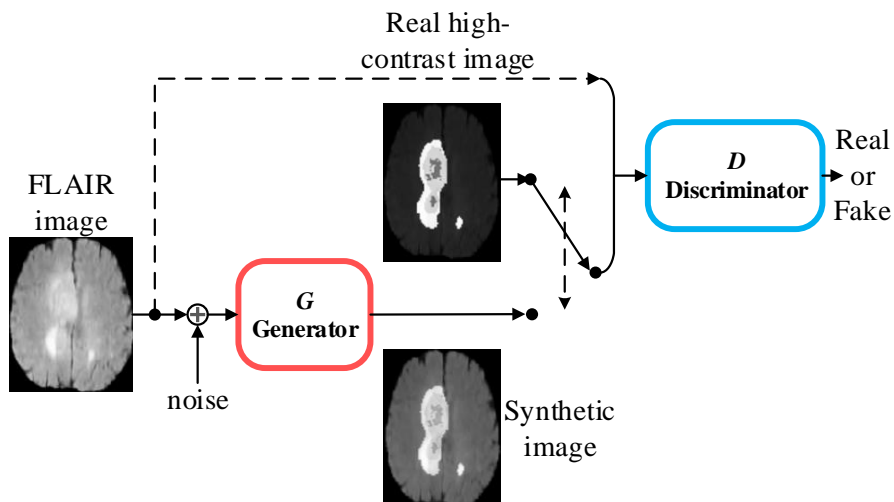


Fig. 2. Deep-learning-based high-contrast synthesis using FLAIR images. After training by GAN, the model outputs the synthetic high tissue contrast images with an inference time of around 20 ms.

size of 128×128 pixels. In implementation details, we follow [11], including the number of epochs, the number of layers, and the kernel sizes. For each subject in the BraTS’19 dataset, we provide a 3D synthetic volume for the next stage, segmentation.

2.2 Synthetic Segmentation

The output volumes from synthetic image generator block are concatenated with real modalities (FLAIR, T1c, and T2) and fed into segmentation block to predict region of interests. The segmentation network allows jointly capturing features from FLAIR, synthetic, T1c, and T2 modality. For the 3D segmentation block, we rely on ensembling the 3D FCN on axial, sagittal, and coronal planes.

3 Experimental Results

3.1 Implementation Details

We implement the proposed design employing the KERAS with 12GB NVIDIA TITAN X GPU. We have scaled image patches to sizes 128×128 pixels for translation. The model is trained through the ADADELTA [19] optimizer (learning rate = 0.9, $\rho = 0.90$, epsilon=1e-5). Dropout is employed to avoid over-fitting over the training ($p_{drop} = 0.4$).

Table 1. DSCs and HD95 of the synthetic segmentation method on BraTS’19 Validation set (training on 335 cases of BraTS’19 training set).

	Dice			Sensitivity			Specificity			HD95 (mm)		
	ET	WT	TC	ET	WT	TC	ET	WT	TC	ET	WT	TC
Mean	76.65	89.65	79.01	76.88	91.32	77.71	99.85	99.39	99.76	4.6	6.9	8.4
Std.	25.86	9.44	23.31	25.35	8.84	26.13	0.23	0.69	0.33	7.2	13.8	12.4
Median	84.73	92.15	89.47	85.47	94.53	90.08	99.93	99.58	99.88	2.2	3.3	4.1
25 quantile	77.88	87.94	74.29	72.82	88.65	73.26	99.82	99.15	99.70	1.4	2.0	2.0
75 quantile	90.21	94.81	93.98	91.97	97.28	95.16	99.98	99.83	99.97	4.1	5.1	10.3

3.2 Datasets

The performance of the proposed method is evaluated on the BraTS’19 dataset, which has two datasets of pre-operative MRI sequences: Training (335 cases) and Validation (125 cases). Each patient is giving $155 \times 240 \times 240$ with four channels: T1, T2, T1c, and FLAIR. In the manual label of BraTS’19, there are three tumor regions: non-enhancing tumor, enhancing tumor, and edema. The evaluation is figured out by CBICA IPP³ online platforms. Metrics computed by the online evaluation platforms in BraTS’19 are Dice Similarity Coefficient (DSC) and the 95th percentile of the Hausdorff Distance (HD95). DSC is considered to measure the union of prediction and manual segmentation. It is measured as $DSC = \frac{2TP}{FP+2TP+FN}$ where TP, FP, and FN are the numbers of true positive, false positive, and false negative detections, respectively.

3.3 Segmentation Results on BRATS’19

Fig. 3 shows examples of brain tumor prediction in LGG and HGG slides on BraTS19 along with corresponding labels, where the subject IDs are "BraTS19-TCIA10-175-1" and "BraTS19-CBICA-APK-1" for LGG and HGG, respectively. The results in Table 1 show that our method performed competitive performance on validation set (125 cases) of BraTS dataset. Results are reported in the online processing platform by BraTS’19 organizer. Moreover, Table 2 reports the average results on 335 training case of the BraTS’19.

4 Overall Survival Prediction Model

BraTS’19 dataset contains 102 gross total resections (GTR) pre-operative scans out of 335 training cases in which the age of patients is available. These subjects are applied for developing a model to predict the overall survival (OS) of the

³ <https://ipp.cbica.upenn.edu>

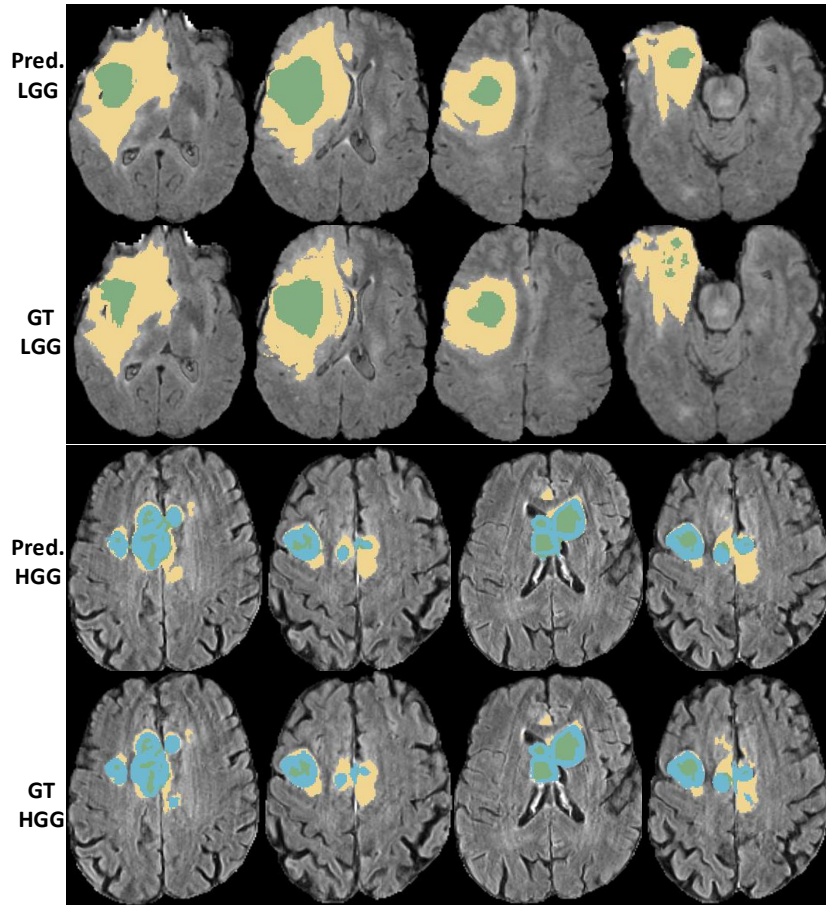


Fig. 3. Segmentation results are overlaid on FLAIR axial slices on BraTS'19 Training Data. The yellow label is edema, blue color means enhancing tumor, and the green one shows the necrotic and non-enhancing tumor core. The first and second rows illustrate LGG brain tumor, prediction (Pred.), and ground truth (GT), respectively. The third and fourth rows are related to HGG tumors. Computed DSCs by the Challenge organizer are reported for the LGG subject as: WT = 96.55% and ET% = 88.85, as well as HGG subject as: TC = 93.80%, WT = 93.97%, and ET = 95.00%.

patient. To this end, we measure the volume of WT, TC, and ET after segmentation to create a feature vector to predict patient OS. We also consider patient's age as an input feature to increase survival prediction accuracy. Thus, we have a 4-dimensional normalized feature vector that scaled between 0 and 1. We train different regression models to predict OS through supervised machine learning, including linear models, regression trees, support vector machines (SVMs) with different kernel functions, Gaussian process regression (GPR) models, and ensembles of trees. We measure root mean square error (RMSE), maximum ab-

Table 2. DSCs and HD95 of the synthetic method on BraTS’19 Training set.

	Dice			Sensitivity			Specificity			HD95 (mm)		
	ET	WT	TC	ET	WT	TC	ET	WT	TC	ET	WT	TC
Mean	79.26	91.65	90.76	84.49	91.89	90.76	99.86	99.51	99.77	3.5	5.7	3.4
Std.	23.96	05.59	7.13	14.46	08.04	08.17	0.178	0.47	0.34	7.3	11.0	4.6
Median	87.04	93.29	92.88	88.12	94.35	93.22	99.92	99.64	99.88	1.4	2.8	2.0
25 quantile	79.49	89.89	88.34	80.69	88.99	87.96	99.831	99.37	99.74	1.0	1.8	1.4
75 quantile	91.54	95.39	95.28	93.78	97.23	96.43	99.975	99.80	99.95	2.2	4.9	3.6

Table 3. Comparison between linear models and regression trees with different hyper-parameters.

	Linear Regression Models				Regression Trees		
	Linear Interactions	Roubust	Stepwise		Fine	Medium	Coarse
RMSE	316.81	375.23	326.76	314.07	377.46	317.35	327.95
MAE	224.24	250.04	220.04	223.36	277.04	237.8	237.38
Pred. speed	2000	6200	7800	7600	4900	19000	19000

Table 4. Comparison between different SVM kernels. Kernel scales for Gaussian (Gaus.) SVM are considered as 0.5, 2, and 8 for Fine, Medium, and Coarse, respectively.

	SVM					
	Linear	Quadratic	Cubic	Fine Gaus.	Medium Gaus.	Coarse Gaus.
RMSE	323.92	354.44	377.65	349.41	341.52	329.36
MAE	220.02	244.46	263.68	234.66	228.45	221.86
Pred. speed	5400	16000	17000	16000	17000	15000

solute error (MAE), and prediction speed during inference (observation/sec) to assess model performance. The 5-fold cross-validation is applied to evaluate these models with four feature vectors.

Table 3 presents linear regression models, including linear, interactions, robust, and stepwise linear models. We also evaluate regression Trees with three minimum leaf sizes, i.e., 4, 12, and 36 in this table.

Table 4 evaluates SVMs models through different Kernel functions and scales. We consider kernel scales 0.5, 2, and 8 for fine, medium, and coarse Gaussian SVM, respectively.

Table 5. Comparison between GPR and ensemble models with several kernel functions. The abbreviation is: (Exp)ponential

	Gaussian Process Regression Models				Ensemble Trees	
	Squared Exp.	Matern	Exp.	Rational Quadratic	Boosted	Bagged
RMSE	332.28	344.9	344.2	332.28	344.16	333.36
MAE	237.93	250.37	249.95	237.93	251.42	240.69
Pred. speed	4900	12000	13000	13000	2600	3400

Table 5 shows GPR and Ensemble Trees models. The former is evaluated with squared exponential, Matern 5/2, exponential, and rational quadratic kernel functions. The boosted Trees and the Bagged Trees are examined for the latter.

Fig. 4 displays predicted response versus subject numbers in BraTS'19. The predictions are accomplished with the stepwise linear regression model.

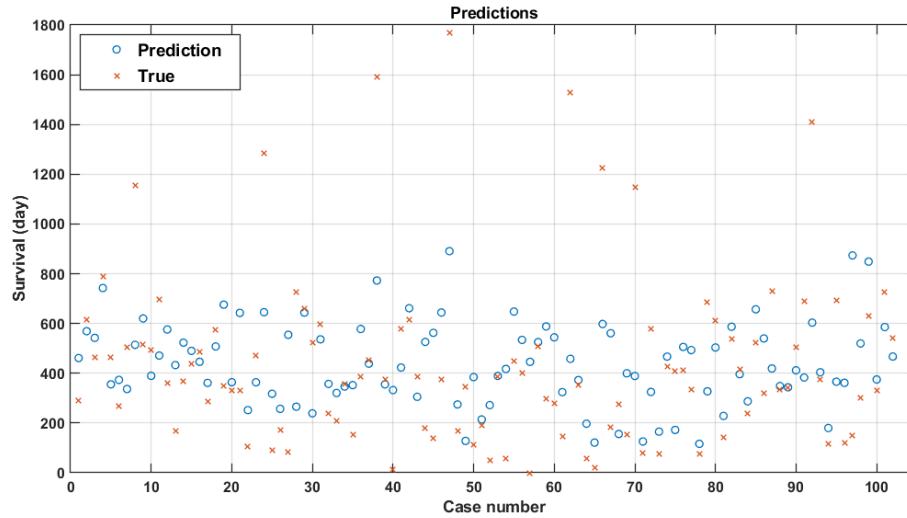


Fig. 4. Survival prediction per day through the stepwise linear regression model. The predicted results versus case number.

Fig. 5 also illustrates predicted response based on three features. We removed age feature to evaluate the effect of this feature on OS task. Table 6 compare RMSE with and without age feature for survival task.

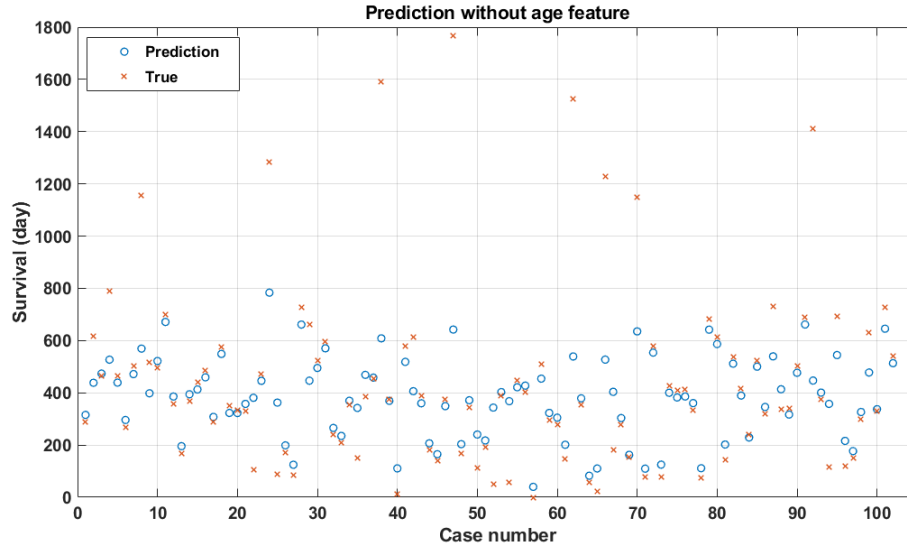


Fig. 5. Survival prediction per day through the stepwise linear regression model. The predicted results versus case number.

Table 6. RMSE with and without age feature.

Feature numbers	Linear	Regression Trees	SVM	Ensemble	GPR
RMSE with age feature	314.07	317.35	323.92	333.36	332.26
RMSE without age feature	357.96	361.45	351.99	362.62	352.53

5 Conclusion

This paper provided a framework for the synthetic segmentation that translated FLAIR MR images into high-contrast synthetic MR ones for segmentation. Synthesizing based on the GAN network empowers our model to decrease the number of real channels in multimodal brain tumor segmentation challenge 2019. We also implemented several regression models to predict the OS of each patient. We found that the stepwise linear model overwhelmed other traditional regression models in terms of RMSE. We also observed that patient age as a distinctive feature in the OS prediction tasks.

6 Acknowledgment

This work was supported partly by National Natural Science Foundation of China (Nos.61871274, 61801305, and 81571758), National Natural Science Foundation of Guangdong Province (No. 2017A030313377), Guangdong Pearl River Talents Plan (2016ZT06S220), Shenzhen Peacock Plan (Nos. KQTD2016053112

051497 and KQTD2015033016 104926), and Shenzhen Key Basic Research Project (Nos. JCYJ20170413152804728, JCYJ20180507184647636, JCYJ20170818142347 251, and JCYJ20170818094109846).

References

1. Bakas, S., Akbari, H., Sotiras, A., Bilello, M., Rozycki, M., Kirby, et al.: Segmentation labels and radiomic features for the pre-operative scans of the TCGA-GBM collection. The Cancer Imaging Archive (2017). <https://doi.org/10.7937/K9/TCIA.2017.KLXWJJ1Q>
2. Bakas, S., Akbari, H., Sotiras, A., Bilello, M., Rozycki, M., Kirby, et al.: Segmentation labels and radiomic features for the pre-operative scans of the TCGA-LGG collection. The Cancer Imaging Archive (2017). <https://doi.org/10.7937/K9/TCIA.2017.GJQ7R0EF>
3. Bakas, S., Akbari, H., Sotiras, A., Bilello, M., Rozycki, M., Kirby, J.S., Freymann, J.B., Farahani, K., Davatzikos, C.: Advancing the cancer genome atlas glioma MRI collections with expert segmentation labels and radiomic features. *Nature Scientific Data* **4**, 170–117 (2017). <https://doi.org/10.1038/sdata.2017.117>
4. Bakas, S., Reyes, M., Jakab, A., Bauer, S., Rempfler, M., Crimi, A., et al.: Identifying the best machine learning algorithms for brain tumor segmentation, progression assessment, and overall survival prediction in the BRATS challenge. arXiv preprint arXiv:1811.02629 (2018)
5. Chen, L., Papandreou, G., Kokkinos, I., Murphy, K., Yuille, A.L.: Deeplab: Semantic image segmentation with deep convolutional nets, atrous convolution, and fully connected crfs. *IEEE Transactions on Pattern Analysis and Machine Intelligence* **40**(4), 834–848 (2018)
6. Goodfellow, I., Pouget-Abadie, J., Mirza, M., Xu, B., Warde-Farley, D., Ozair, S., Courville, A., Bengio, Y.: Generative adversarial nets. In: *Advances in Neural Information Processing Systems*. pp. 2672–2680 (2014)
7. Hamghalam, M., Ayatollahi, A.: Automatic counting of leukocytes in giemsa-stained images of peripheral blood smear. In: *2009 International Conference on Digital Image Processing*. pp. 13–16 (2009). <https://doi.org/10.1109/ICDIP.2009.9>
8. Hamghalam, M., Motameni, M., Kelishomi, A.E.: Leukocyte segmentation in giemsa-stained image of peripheral blood smears based on active contour. In: *2009 International Conference on Signal Processing Systems*. pp. 103–106 (2009). <https://doi.org/10.1109/ICSPS.2009.36>
9. Harley, A.W., Derpanis, K.G., Kokkinos, I.: Segmentation-aware convolutional networks using local attention masks. In: *2017 IEEE International Conference on Computer Vision (ICCV)*. pp. 5048–5057 (2017)
10. Hatami, T., et al.: A machine learning approach to brain tumors segmentation using adaptive random forest algorithm. In: *2019 5th Conference on Knowledge Based Engineering and Innovation (KBEI)*. pp. 076–082 (2019). <https://doi.org/10.1109/KBEI.2019.8735072>
11. Isola, P., Zhu, J., Zhou, T., Efros, A.A.: Image-to-image translation with conditional adversarial networks. In: *2017 IEEE Conference on Computer Vision and Pattern Recognition (CVPR)*. pp. 5967–5976 (2017)
12. Long, J., Shelhamer, E., Darrell, T.: Fully convolutional networks for semantic segmentation. In: *2015 IEEE Conference on Computer Vision and Pattern Recognition (CVPR)*. pp. 3431–3440 (2015)

13. Menze, B.H., Jakab, A., Bauer, S., Kalpathy-Cramer, J., Farahani, K., et al.: The multimodal brain tumor image segmentation benchmark (BRATS). *IEEE Transactions on Medical Imaging* **34**(10), 1993–2024 (2015). <https://doi.org/10.1109/TMI.2014.2377694>
14. Najrabi, D., et al.: Diagnosis of astrocytoma and globalastom using machine vision. In: 2018 6th Iranian Joint Congress on Fuzzy and Intelligent Systems (CFIS). pp. 152–155 (2018). <https://doi.org/10.1109/CFIS.2018.8336661>
15. Ronneberger, O., Fischer, P., Brox, T.: U-net: Convolutional networks for biomedical image segmentation. In: *Medical Image Computing and Computer-Assisted Intervention*. pp. 234–241. Springer (2015)
16. Roy, A.G., Conjeti, S., Sheet, D., Katouzian, A., Navab, N., Wachinger, C.: Error corrective boosting for learning fully convolutional networks with limited data. In: *Medical Image Computing and Computer Assisted Intervention*. pp. 231–239. Springer (2017)
17. Soleimany, S., et al.: A novel random-valued impulse noise detector based on mlp neural network classifier. In: 2017 Artificial Intelligence and Robotics (IRA-NOPEN). pp. 165–169 (2017). <https://doi.org/10.1109/RIOS.2017.7956461>
18. Soleymanifard, M., Hamghalam, M.: Segmentation of whole tumor using localized active contour and trained neural network in boundaries. In: 2019 5th Conference on Knowledge Based Engineering and Innovation (KBEI). pp. 739–744 (2019). <https://doi.org/10.1109/KBEI.2019.8735050>
19. Zeiler, M.D.: ADADELTA: an adaptive learning rate method. *CoRR* **abs/1212.5701** (2012)